Quasiadiabatic approach for laser-induced single-bubble sonoluminescence

Rasoul Sadighi-Bonabi,[1,*] Fatemeh Razeghi,[1] Homa Ebrahimi,[1] Shadi Fallahi,[1,2] and Erik Lotfi[3]
[1]*Department of Physics, Sharif University of Technology, 11365-91 Tehran, Iran*
[2]*Department of Physics, Islamic Azad University Science and Research Branch, 1477893855 Tehran, Iran*
[3]*Department of Optics and Laser, University of Bonab, 1783892612 Bonab, Iran*
(Received 23 May 2011; revised manuscript received 5 November 2011; published 4 January 2012)

The luminescence parameters of laser-induced bubble in the presence of an acoustic field in water are studied. A comparison is made between parameters such as bubble radius, interior temperature, and pressure of the bubble induced by laser and an acoustic field influenced by different driving pressure amplitudes. It is found that the bubble volume induced by laser at the collapse instant is more than 10^6 times larger than the one induced by an acoustic field. It is also noticed, by increasing the driving pressure amplitude, the bubble radius decreases in both cases, however, the bubble interior pressure and temperature increase.

DOI: 10.1103/PhysRevE.85.016302 PACS number(s): 47.55.dp, 43.35.Hl, 47.55.dd

I. INTRODUCTION

One of the most interesting topics in physics of fluids is the generation of a bubble created in different liquids and its oscillations. Generally, to create bubbles a sound field is applied, which normally leads to the production of multibubble sonoluminescence (MBSL) and deals with interaction of several bubbles and investigating of their dynamics [1,2]. Single-bubble sonoluminescence (SBSL) is also produced in special exerting conditions [3–5]. Various aspects of SBSL and MBSL are studied, including intensity and spectrum of the emitted light [6–8] and its dependency on the ambient parameters [9,10], the dissolved gas in liquids [11], the phase diagrams [12,13], the pulse width [14,15], the conditions of bubble stability [16,17], and the modification of the initial Rayleigh-Plesset equation considering various effects of the medium such as compression viscosity of the liquids [2,5,18].

Some other ways are also used to produce transient cavitation bubbles named as single cavitation bubble luminescence (SCBL), such as electrical discharge [19,20], syringe injection of gas into a venture flow field [21], or colloidal particle suspensions [22]. In recent years, the applications of a focused laser beam have become a very attractive way of obtaining SCBL due to its unique features [23,24]. In this method, a laser pulse is focused into a transparent buffer liquid-like water, and bubbles which are induced by the laser are so-called laser-induced single cavitation bubble luminescence (LI-SCBL). Optical breakdown due to the laser radiation occurs, followed by mechanical effects such as emission shock wave and cavitation bubble expansion. During the optical breakdown process, the energy of the laser pulse is transmitted in the medium, absorbed, scattered, or reflected [25,26]. Part of the laser energy that is absorbed in the transparent media goes into the cavitation bubble energy, the shock-wave energy, the plasma radiation, and the evaporation energy [27]. Due to the increase of the liquid pressure, the bubble collapses violently and eventually emits a shock wave and a flash of light. The bubble's oscillation is estimated to have only a few rebounds and after that, the bubble expands again and has several oscillations [28]. Also the duration of flash light for LI-SCBL is of the order of a few nanoseconds and the photon numbers emitted from these bubbles are of the order of magnitudes greater than was observed in single-bubble sonoluminescence [23,29]. The order of emitted photons of bubbles induced by laser is about 10^8 photons and it is more than the one produced from the other methods [23]. Bubbles produced by LI-SCBL are reported to have maximum radii 10–30 times larger than the SBSL [23,30]. This results in more than three orders of magnitude radiating species in the bubble than the earlier SBSL-produced process. Larger bubble volume makes the LI-SCBL method even more attractive, especially for the recent application of sound amplification by stimulated emission of radiation (SASER) due to its larger SASER cavity [31,32]. In spite of the larger bubble radius induced by laser, the bubble interior pressure and temperature are smaller than the ones for SBSL. Therefore, it is not a suitable environment for sonoluminescence applications for fusion that have been recently explored [33,34]. However, the obtained temperature is sufficient for achieving the required population inversion and producing high-power SASER radiation. As mentioned, some useful analyses of LI-SCBL are reported in the literature. However, a complete model to investigate the systematic behavior of the bubble parameters has never been introduced.

Generally, various models have been introduced to investigate the evolution of the processes inside a sonoluminescence bubble such as isothermal, hydrochemical, and quasiadiabatic models [35–39]. In the isothermal model some important parameters such as temperature cannot be calculated [2,13,36]. In the hydrochemical model, heat and mass transfer between bubble and environment fluid and chemical reactions are considered. In this model most of the chemical reactions are endothermic. However, due to the complication of the process, many chemical reactions are ignored [5]. Therefore, the calculated temperature in the hydrochemical model is less than that in the quasiadiabatic model [5]. In the quasiadiabatic model, the mentioned evolutions at the moment of collapse will be assumed adiabatic due to the rapid compression of the bubble wall and it is isothermal in the rest of the cycle [40,41]. All of these models are applied to SBSL, MBSL, and moving SBSL [2,13,36,37]. A similar discussion for LI-SCBL has not been proposed before.

In this work, the quasiadiabatic model is used to study the fluctuation of a single-bubble sonoluminescence in the

*sadighi@sharif.ir

presence of a laser pulse and a sound field. By using this model, the complete cycle of bubble movement is represented for LI-SCBL in the presence of the acoustic field. Based on the mentioned model, some important bubble parameters such as interior pressure and temperature are investigated. By comparing the obtained results for LI-SCBL in the presence of the acoustic field, it is found that the maximum and minimum bubble radii are about 10 and 100 times larger than the ones for the SBSL, respectively. This approach and achievement are discussed in detail.

II. THE MODEL

Using the Rayleigh-Plesset equation, the oscillations of a transient cavitation bubble induced by laser in the presence of the sound field is studied. Due to the presence of the laser, the liquid is assumed to behave as a compressible fluid. To model the oscillation, the bubble is considered in one acoustical cycle from $t = 0$ to $t = T$ (the period of the sound field). This model is based on the quasiadiabatic process, which is almost adiabatic near a collapse time due to the very short collapsing time and it is isothermal during the other cycle time [2,37]. In this condition the bubble oscillations can be described by the following Rayleigh-Plesset equation [42]:

$$(1 - \dot{R}/C)R\ddot{R} + 3/2(1 - \dot{R}/3C)\dot{R}^2 = (1 + \dot{R}/C)(P_l - P_a - P_0)/\rho + (R/\rho C)dP_l/dt, \quad (1)$$

where R, $\dot{R}$, $\ddot{R}$, ρ, and C are the bubble radius, the bubble wall velocity, the bubble wall acceleration, the density of the liquid, and the speed of sound on the bubble wall, respectively. P_0 indicates the atmospheric pressure and P_a denotes the acoustic driving term, which is supposed to be a sinusoidal driving pressure [43]:

$$P_a(t) = P_A \sin(2\pi f t), \quad (2)$$

where P_A and f are the amplitude and the frequency of the driving acoustic field, respectively. In the previous works, the frequency of the sound field for water was selected to be about 30 kHz [13]. In the presence of laser and an acoustic field to create a bubble with its fluctuations, the magnitude of frequency is less than that in the SBSL and approximately between 4.5 and 9 kHz [43]. This is due to the fact that part of the energy is supplied by the laser. Therefore, a lower frequency is needed to produce the bubble and its oscillation. In the presence of the laser, the induced pressure of the laser that is followed by shock wave is so great that the environment acts as a compressible fluid. But for SBSL the driving pressure amplitude is not so great and the fluid could not be considered as compressible. Therefore, the speed of sound in water is constant and is equal to $C_0 = 1483$ m/s. Therefore, all the equations are the same except for the sound velocity. The effect of the compressibility in the variation of the sound velocity is shown as the following [44]:

$$C = C|_{r=R} = \sqrt{dP_l/d\rho}|_{r=R}. \quad (3)$$

The liquid pressure on the bubble wall, in the quasiadiabatic process is expressed with [5]

$$P_l(R,\dot{R}) = P_g - \frac{2\sigma}{R} - \frac{4\mu\dot{R}}{R}. \quad (4)$$

Here μ and σ are fluid kinematic viscosity and surface tension. P_g is the gas pressure in the bubble [35]:

$$P_g = \left(P_0 + \frac{2\sigma}{R_0}\right)\left(\frac{R_0^3 - a^3}{R(t)^3 - a^3}\right)^{\gamma}. \quad (5)$$

R_0 is the ambient bubble radius which is induced by laser, $a = R_0/8.86$ indicates a hard-core van der Waals term for water vapor [45], and γ is the polytropic exponent and describes the degree of isothermality or adiabaticity during the bubble cycle [46].

One can obtain an equation for the variation of the gas temperature:

$$\dot{T} = -[\gamma(R,\dot{R},T) - 1]\frac{3R^2\dot{R}}{R^3 - a^3}T - \chi_g\frac{T - T_0}{R^2}. \quad (6)$$

In this equation, T, T_0, and χ_g are the gas temperature, the ambient temperature, and the thermal diffusion of the gas inside the bubble [46,47]. $\gamma(R,\dot{R},T)$ is a function of R, $\dot{R}$, and T as follows [48]:

$$\gamma(\mathrm{Pe}) = 1 + (\Gamma - 1)\exp\left(-\frac{A}{(\mathrm{Pe})^D}\right), \quad (7)$$

where A and D are constant and Γ is the adiabatic exponent and equal to $\Gamma = 5/3$ for argon [48]. Pe indicates Pèclet number and yields [47]

$$\mathrm{Pe} = \mathrm{Pe}(t) = \frac{R(t)|\dot{R}(t)|}{\chi_g(R,T)}. \quad (8)$$

According to Eq. (7), $\gamma(\mathrm{Pe})$ is related to Pèclet number and is used for a strong collapse of a sonoluminescence bubble. By considering heat diffusion during the bubble's expansion, the isothermal behavior can be taken into account and due to the low speed of the bubble wall, the Pèclet number is small: $\gamma(\mathrm{Pe} \to 0) \to 1$. While during rapid comparison, there is a large increase in the bubble temperature, when Pe becomes large the system deviates significantly from isothermal behavior$\gamma(\mathrm{Pe} \to \infty) \to 5/3$ [35,46].

In the presence of a laser, the surrounded liquid acts as a compressible fluid so the pressure of the liquid is a function of density as shown by the following:

$$\frac{P_l(R,\dot{R}) + B}{P_0 + B} = (\rho/\rho_0)^n. \quad (9)$$

n and B are constants and depend on the type of fluids [43].

In the hydrochemical model, gas pressure in the bubble is expressed with [49]

$$P_g = \frac{N_{\mathrm{tot}}k_B T_g}{V - N_{\mathrm{tot}}B}. \quad (10)$$

Here N_{tot}, k_B, and V are the total number of particles inside the bubble, Boltzmann's constant, and the bubble volume, respectively. $B = 5.1 \times 10^{-29}$ m^3 is the hard-core parameter which assumed to be equal for all particles.

Variation of the gas temperature in the hydrochemical model is calculated from [49]

$$\dot{T}_g\frac{\partial e_{\mathrm{th},j}}{\partial T_g}N_j = \dot{Q} - P_g\dot{V} - \sum_j e_{\mathrm{th},j}\dot{N}_j + \dot{E}_{\mathrm{chem}} + \sum_j h_{w,j}\dot{N}_j^d. \quad (11)$$

T_g shows the gas temperature in the hydrochemical model, N_j indicates the vapor species j inside the bubble, and N_j denotes the rate of change in vapor species j inside the bubble. Q and V are the rate of heat transfer and bubble volume, respectively. The quantity $\dot{E}_{\rm chem}$ denotes the rate of change in the chemical energy of the bubble due to reactions considered in the model. $h_{w,j} = [1 + (f_j/2)]k_B T_0$ is the molecular enthalpy of the particles of species j at the bubble wall temperature T_0, with f_j as its number of translational and rotational degrees of freedom. Because of mass diffusion and chemical reactions at the collapse time, the number of particles in the bubble changes with time and five more molecules and chemical radicals are produced inside the bubble. In Eq. (11) $\dot{N}_j^d$ is the diffusion rate of particles of species j and is equal to [49]

$$\dot{N}_j^d = -4\pi R^2 D \frac{n_j}{l_d}, \quad l_d = \min\left(\sqrt{\frac{RD}{|\dot{R}|}}, \frac{R}{\pi}\right). \tag{12}$$

D is the diffusion constant given by $D = D_0(n_0/n_{\rm tot})$, where $D_0 = 23.55 \times 10^{-6}$ m^2/s. $n_{\rm tot}$ and n_0 are the instantaneous total number density of the bubble and equilibrium concentration of the bubble, respectively. Here the quality l_d is the thickness of the diffusive boundary layer.

$e_{{\rm th},j}$ is thermal energy of the molecule j given by [49]

$$e_{{\rm th},j} = \frac{f_j}{2} k T_g + \sum_l \frac{k\Theta_{j,l}}{e^{\Theta_{j,l}/T_g} - 1}. \tag{13}$$

$\Theta_{j,l}$, $l = 1, \ldots, l_{\rm max}$, denotes the various characteristic vibration temperatures of the particle species j. $l_{\rm max} = 3m - 6$ except for diatomic molecules, which is $l_{\rm max} = 3m - 5$, where m is the number of particle species. The different values for $\Theta_{j,l}$ correspond to characteristic vibration temperatures (in K) of the particle species j listed in Table I.

The chemical reactions inside the bubble in liquid water at the collapse time are as follows [50]:

$$\begin{aligned}
O + O + Ar &\leftrightarrow O_2 + Ar,\\
O + H + Ar &\leftrightarrow OH + Ar,\\
O + H_2 &\leftrightarrow H + OH,\\
H + O_2 &\leftrightarrow O + OH,\\
H + H + Ar &\leftrightarrow H_2 + Ar,\\
H + OH + Ar &\leftrightarrow H_2O + Ar,\\
OH + H_2 &\leftrightarrow H + H_2O,\\
OH + OH &\leftrightarrow O + H_2O.
\end{aligned}$$

TABLE I. The characteristic vibration temperatures (in K) of the various particle species in the hydrochemical model and their numbers of translation and rotational degrees of freedom [49].

Species	H_2	H	O	O_2	OH	H_2O	Ar
$\Theta_{j,1}$	6325			2273	5370	2295	
$\Theta_{j,2}$						5255	
$\Theta_{j,3}$						5400	
f_j	5	3	3	5	5	6	3

III. NUMERICAL RESULTS

In this section, the numerical results of the bubble simulation are presented. The calculations are carried out by using the simulation code with the Runge-Kutta algorithm. The parameters are given as $C_0 = 1483$ m/s, $P_0 = 1.013$ bars, $\rho_0 = 998$ kg/m, $\sigma = 0.072\,75$ N/m, $\mu = 0.001$ N s/m^3. n and B are constants and for water are equal to $n = 7$ and $B = 3122$ bars [43]. A and D in Eq. (7) are constant and equal to $A = 5.8$, $D = 0.6$. The initial gas temperature is selected to be 293.16 K. To induce bubbles, a Nd:YAG laser pulse with FWHM of 8 ns at a wavelength of 1064 nm is used in addition to a sound field with frequency $f = 6000$ Hz. The pulse energy for nanosecond pulses is between 1.8 and 3 mJ. The part of the laser energy that is absorbed in the transparent media goes into the cavitation bubble energy, the shock-wave energy, the plasma radiation, and the evaporation energy. The parameters mentioned in this work are similar to the reported experimental values where in this condition the absorbed laser energy is about 91%, where almost 25% of this energy is consumed to produce the bubble [27], and this is what we have considered in our calculations to compare the obtained results with the reported experimental measurements by using lasers with the mentioned parameters.

In Figs. 1–3, the difference between the bubble radius, the interior pressure, and the temperature for a bubble in a sound field with and without laser radiation is denoted. In Figs. 4–6, the variations of these parameters are investigated for three driving pressure amplitudes.

Figure 1 indicates the bubble radius in one cycle in the luminescence parameter regime for two conditions: (a) in LI-SCBL in the presence of the acoustic field for the luminescence parameter regime $P_a = 2.0$ bars, $R_0 = 1.2 \times 10^{-4}$ m, and $f = 6000$ Hz (solid line), and (b) in SBSL with the driving pressure amplitude, the ambient bubble radius, and the frequency equal to $P_a = 1.6$ bars, $R_0 = 2 \times 10^{-6}$ m, and

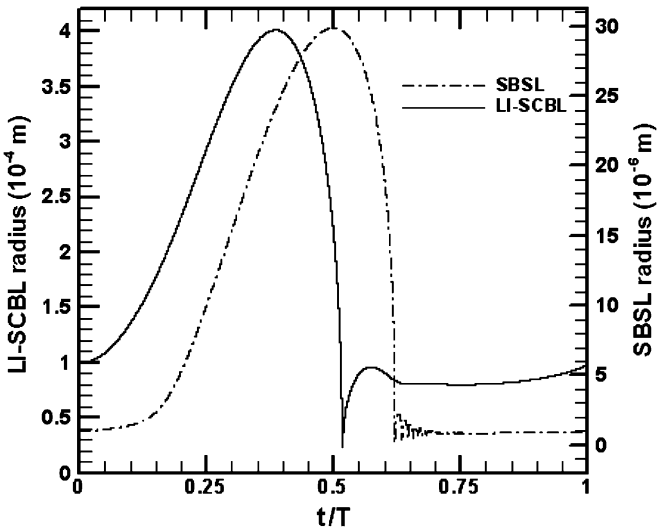

FIG. 1. The bubble radius as a function of time for two models: LI-SCBL in the presence of the acoustic field (solid line), with $P_a = 2.0$ bars, $R_0 = 1.2 \times 10^{-4}$ m, and $f = 6000$ Hz, and SBSL (dash-dotted line), with $P_a = 1.6$ bars, $R_0 = 2 \times 10^{-6}$ m, and $f = 26\,500$ Hz.

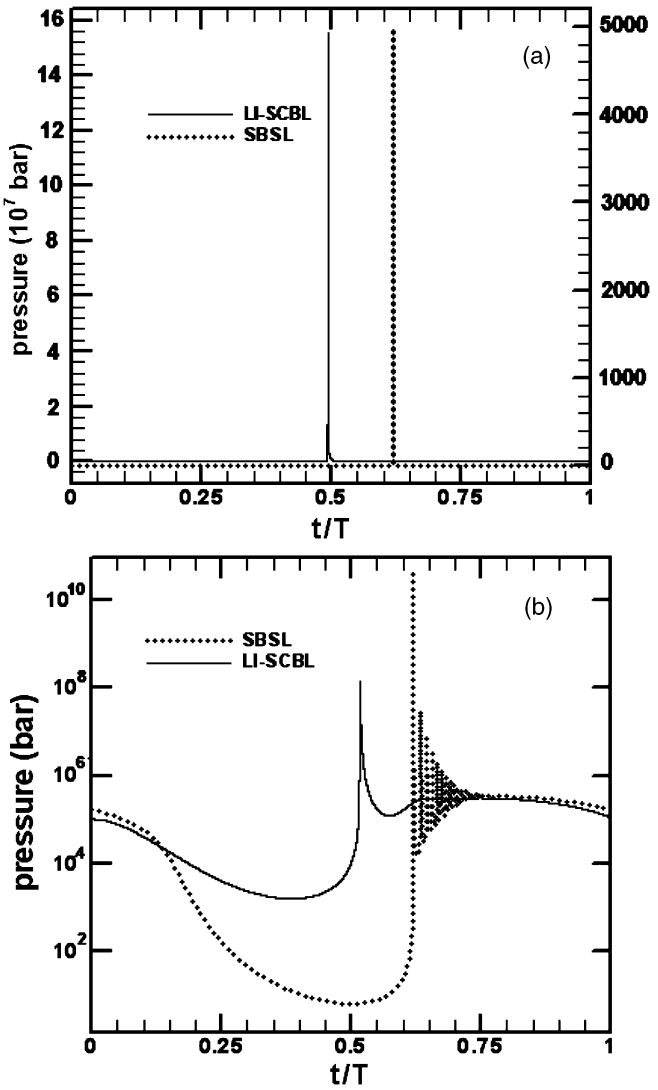

FIG. 2. Variation of bubble interior pressure as a function of time (a) for two models: LI-SCBL in the presence of the acoustic field (solid line) with $P_a = 2.0$ bars, $R_0 = 1.2 \times 10^{-4}$ m, and $f = 6000$ Hz, and SBSL (dash-dotted line) $P_a = 1.6$ bars, $R_0 = 2 \times 10^{-6}$ m, and $f = 26\,500$ Hz. (b) Variation of bubble interior pressure as a function of time with semilogarithmic scale for LI-SCBL in the presence of the acoustic field and SBSL.

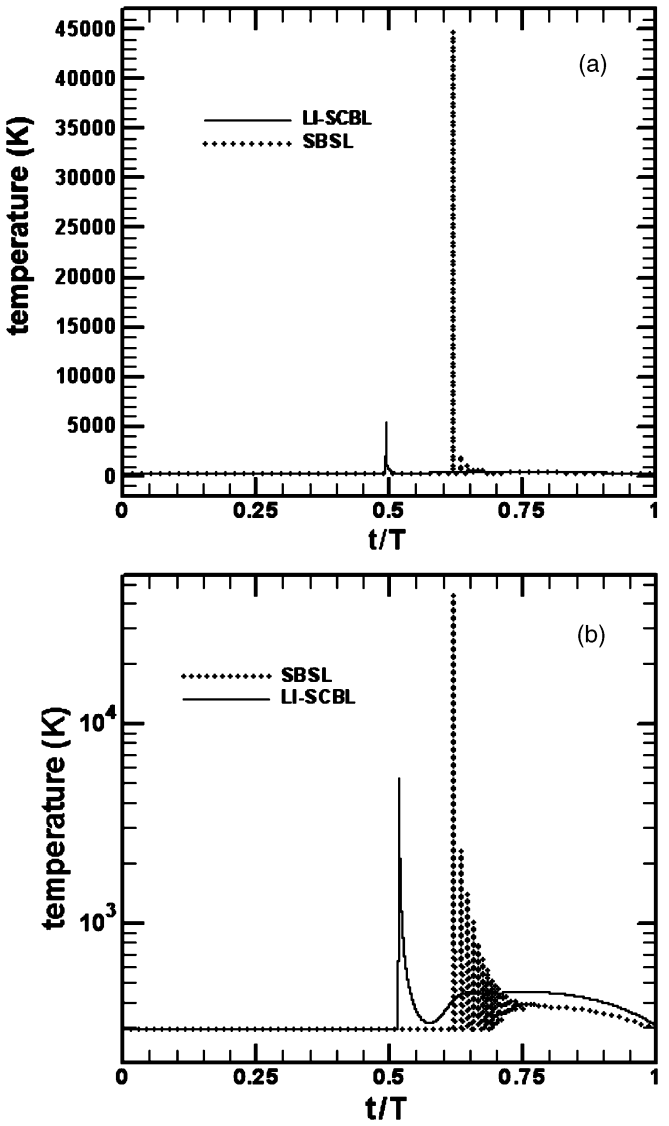

FIG. 3. Variation of bubble interior temperature as a function of time (a) for two modes: LI-SCBL in the presence of the acoustic field (solid line), with driving pressure amplitude, the ambient bubble radius, and the frequency equal to $P_a = 2.0$ bars, $R_0 = 1.2 \times 10^{-4}$ m, and $f = 6000$ Hz, and SBSL (dash-dotted line), with driving pressure amplitude, ambient bubble radius, and frequency equal to $P_a = 1.6$ bars, $R_0 = 2 \times 10^{-6}$ m, and $f = 26\,500$ Hz. (b) Variation of the bubble interior temperature as a function of time with semilogarithmic scale for LI-SCBL in the presence of the acoustic field and SBSL.

$f = 26\,500$ Hz, respectively (dash-dotted line). It should be noted that the left scale chart is based on 10^{-4} m, which shows the oscillation period of a bubble in the condition of LI-SCBL in the presence of the acoustic field, but the right scale chart is based on 10^{-6} m, which shows the oscillation period of SBSL. Diagrams show that the maximum of the bubble radius for LI-SCBL in the presence of the acoustic field is more than ten times larger than the maximum of the bubble radius for SBSL. But it is observed that the difference between the maximum and the minimum bubble radius is larger for SBSL than the one related to LI-SCBL in the presence of the acoustic field. As shown in the diagram, in SBSL, the bubble radius reaches more than 30 times its initial radius, while in LI-SCBL in the presence of the acoustic field the maximum of the bubble radius is almost five times its initial radius. In addition, LI-SCBL in the presence of the acoustic field reaches the collapse time faster and fewer afterbounces are observed due to its larger bubble radius. The bubble radius induced by laser in this simulation is consistent with the experimental results [51].

Figure 2(a) represents the pressure inside the bubble for LI-SCBL in the presence of the acoustic field and SBSL, for the same parameters mentioned in Fig. 1. In this figure the left scale chart is based on 10^7 bars, which shows the pressure inside the bubble of LI-SCBL in the presence of the acoustic field and the right scale charter presents the bubble evolution for SBSL. As shown, the pressure inside the bubble of SBSL is more than 300 times larger than that in the bubble interior

pressure of LI-SCBL in the presence of the acoustic field. This is due to a large difference between the maximum and the minimum of the bubble radius, as mentioned in Fig. 1, and the smaller collapsing time in SBSL rather than in LI-SCBL in the presence of the acoustic field. By comparing Figs. 1 and 2, it is seen that the peak of the interior gas pressure is at the collapse time, and the time difference between these two peaks is associated with the time delay in their collapse time, as shown in Fig. 1. Figure 2(a) presented with semilogarithmic scale in Fig. 2(b) to indicate the structure. During the bubble's expansion, the bubble interior pressure decreases until it reaches its minimum amount in the maximum radius. By rapid compression, the bubble interior pressure increases violently and reaches its maximum amount at the collapse time. The several peaks in SBSL are related to bubble rebounds that are shown in Fig. 1, whereas there is only one peak for LI-SCBL in the presence of the acoustic field.

In the assumed quasiadiabatic model, there is no heat and particle exchange in the collapse time and there is a huge accumulation of energy in the gas bubble. Therefore, a more intense collapse results in the higher interior pressure and temperature. As shown in Fig. 3(a), the temperature inside the bubble in SBSL reaches 45 000 K, almost nine times larger than the one for LI-SCBL in the presence of the acoustic field. That is due to the sharp and intense collapse

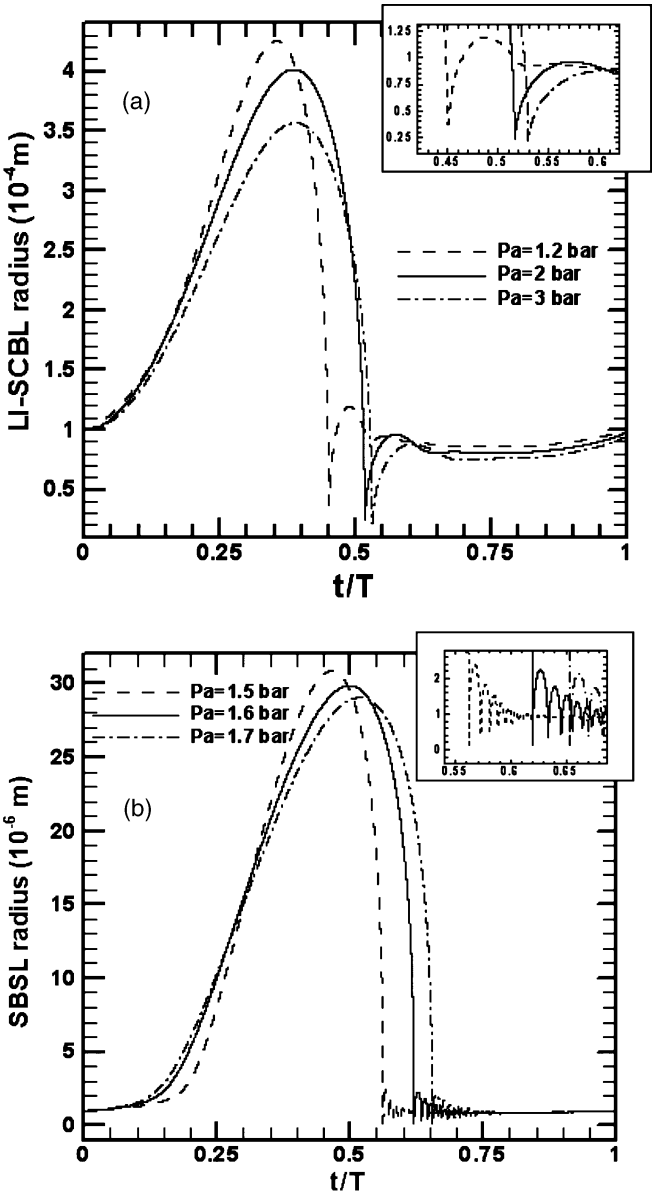

FIG. 4. Comparison of the bubble radius for three driving pressures in two modes: (a) LI-SCBL in the presence of the acoustic field in the luminescence parameter regime $P_a = 1.2$ bars, with $R_0 = 0.4 \times 10^{-4}$ m, $P_a = 2$ bars with $R_0 = 1.2 \times 10^{-4}$ m, and $P_a = 3$ bars with $R_0 = 2.1 \times 10^{-4}$ m, and (b) SBSL in the luminescence parameter regime $P_a = 1.5$ bars with $R_0 = 1.3 \times 10^{-6}$ m, $P_a = 1.6$ bars with $R_0 = 2 \times 10^{-6}$ m, and $P_a = 1.7$ bars with $R_0 = 2.5 \times 10^{-6}$ m.

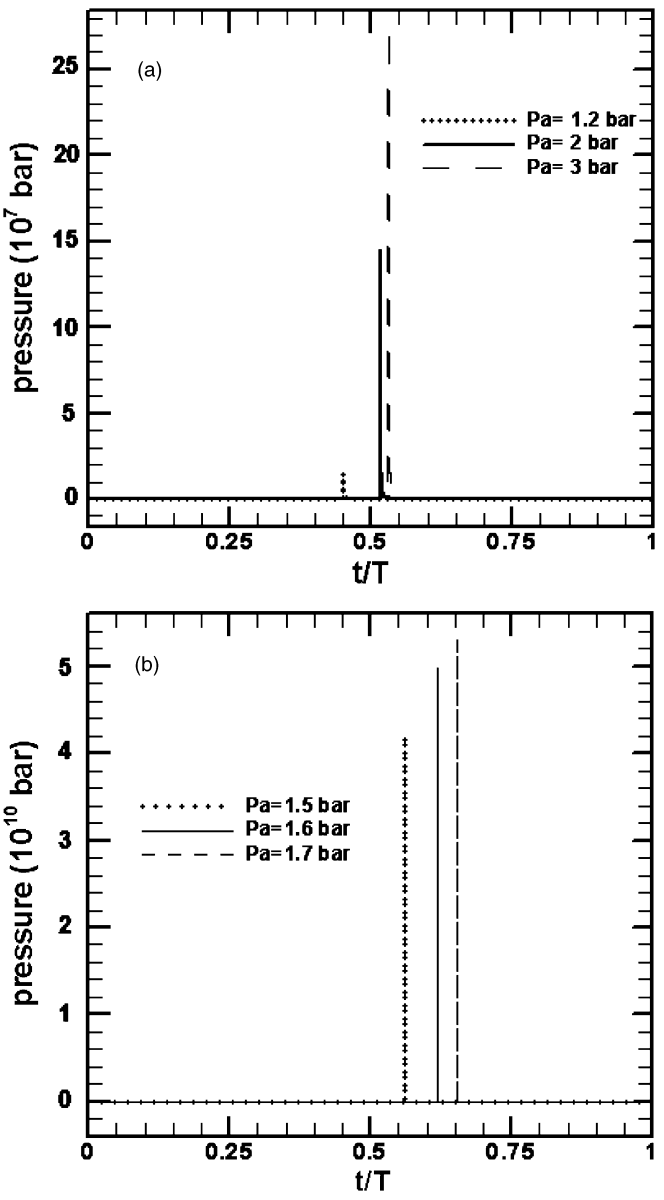

FIG. 5. Compare the bubble interior pressure as a function of time for different driving pressure amplitudes as indicated in Fig. 4 in two modes: (a) LI-SCBL in the presence of the acoustic field and (b) SBSL.

and higher gas pressure in SBSL rather than LI-SCBL in the presence of the acoustic field. Moreover, one can see several peaks in the temperature profile for SBSL that are related to the bubble rebounds, whereas there is only one peak for LI-SCBL in the presence of the acoustic field. It is shown that although the maximum radius of the sonoluminescing bubble in LI-SCBL in the presence of the acoustic field is larger than that in the SBSL, because of the more intense and the shorter collapse time in SBSL, the bubble interior gas pressure and temperature is larger than that in the LI-SCBL in the presence of the acoustic field. Therefore, the presence of the laser beam beside the acoustic field results in a larger and colder sonoluminescence bubble. The bubble interior temperature in this work is consistent with the experimental results [51]. Figure 3(a) presented with semilogarithmic scale to indicate the structure. Before the bubble reaches its maximum radius, the bubble interior temperature is constant. At the collapse time, due to rapid compression, the temperature increases violently. The several peaks in SBSL are related to bubble rebounds that are shown in Fig. 1, whereas there is only one afterbounce for LI-SCBL in the presence of the acoustic field.

In Figs. 4–6, the effect of the driving pressure is compared for LI-SCBL in the presence of the acoustic field and SBSL. To ensure the bubble stabilities by changing the pressure amplitude, the bubble initial radius is changed [52]. It should be realized that in each case an appropriate phase diagram is used [53,54]. The achieved theoretical results are shown in Figs. 4–6.

Figure 4 denotes the oscillation of the bubble for three driving pressure amplitudes and suitable initial bubble radii; one can see the following cases: (a) LI-SCBL in the presence of the acoustic field in the luminescence parameter regime $P_a = 1.2$ bars with $R_0 = 0.4 \times 10^{-4}$ m, $P_a = 2$ bars with

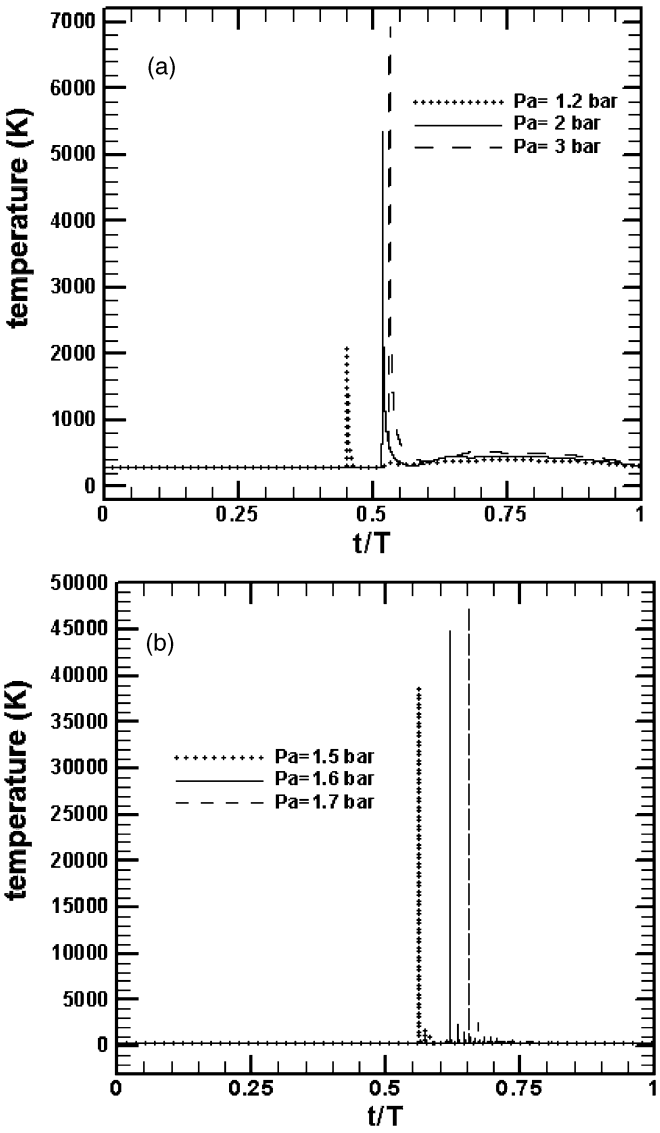

FIG. 6. Temperature changes at the collapse time for different driving pressure amplitudes as indicated in Fig. 4 in two modes: (a) LI-SCBL in the presence of the acoustic field and (b) SBSL.

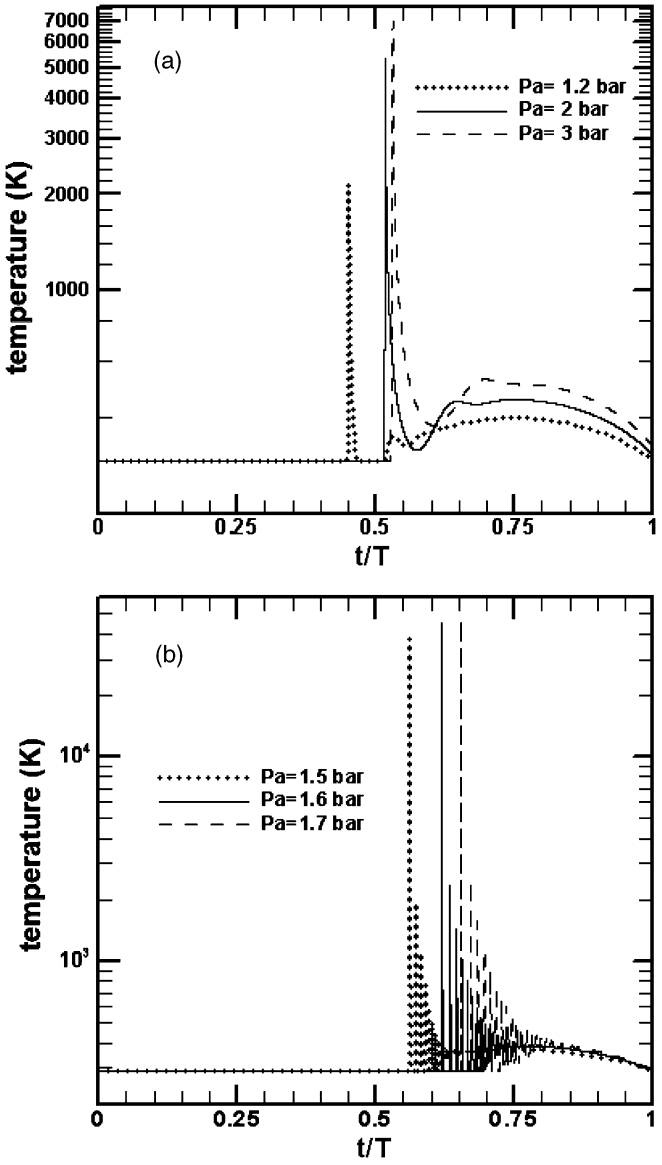

FIG. 7. Bubble interior temperature variations for different driving pressure amplitudes as indicated in Fig. 6 in two modes: (a) LI-SCBL in the presence of the acoustic field and (b) SBSL with logarithm scale.

$R_0 = 1.2 \times 10^{-4}$ m, and $P_a = 3$ bars with $R_0 = 2.1 \times 10^{-4}$ m, and (b) SBSL in the luminescence parameter regime $P_a = 1.5$ bars with $R_0 = 1.3 \times 10^{-6}$ m, $P_a = 1.6$ bars with $R_0 = 2 \times 10^{-6}$ m, and $P_a = 1.7$ bars with $R_0 = 2.5 \times 10^{-6}$ m. As shown in the diagrams, by increasing the driving pressure amplitude, the decreased bubble maximum radius occurs later. By comparing Figs. 4(a) and 4(b), one can notice that in LI-SCBL in the presence of the acoustic field, the minimum bubble radius at the collapse time is more sensitive to the pressure change than in SBSL.

In Fig. 5, a comparison is made to investigate the effects of the driving pressure amplitude on the interior pressure of the gas bubble in LI-SCBL in the presence of the acoustic field and SBSL. The applied pressure amplitude and the initial bubble radius are similar to the ones mentioned in Fig. 4. The increase of the driving pressure results in an increase of the bubble interior pressure for both cases, but the gas pressure change in LI-SCBL in the presence of the acoustic field is more than that in the SBSL. However, the applied pressure amplitude steps of the LI-SCBL in the presence of the acoustic field are slightly higher than the other one. By increasing the driving pressure amplitudes, the bubble size decreases and its pressure increases. It can be noticed that the pressure in Fig. 5(b) is almost 200 times larger than that in Fig. 5(a). By increasing the driving pressure amplitude in LI-SCBL in the presence of the acoustic field from 1.2 bars to 2 bars, the pressure increases to about 13×10^7 bars. A similar increment occurs as the pressure amplitude increases from 2 bars to 3 bars and this is a considerable amount of pressure change in the bubble interior. The driving pressure amplitude for the SBSL increases from 1.5 bars to 1.6 bars and finally to 1.7 bars. These changes increase the bubble interior pressure from 4×10^{10} bars to 5×10^{10} bars and finally to 7×10^{10} bars. It can be realized that the order of pressure increases almost two times. Although the order of pressure inside the SBSL is about 200 times larger than LI-SCBL in the presence of the acoustic field, the gas pressure change in LI-SCBL in the presence of the acoustic field is more in the case of SBSL. As a consequence, in LI-SCBL in the presence of the acoustic field the bubble interior pressure is more sensitive to the applied pressure amplitude.

Figure 6 indicates the temperature variations of the interior bubble in the two mentioned situations by various driving pressure amplitudes and proper ambient bubble radius (a) in LI-SCBL in the presence of the acoustic field by

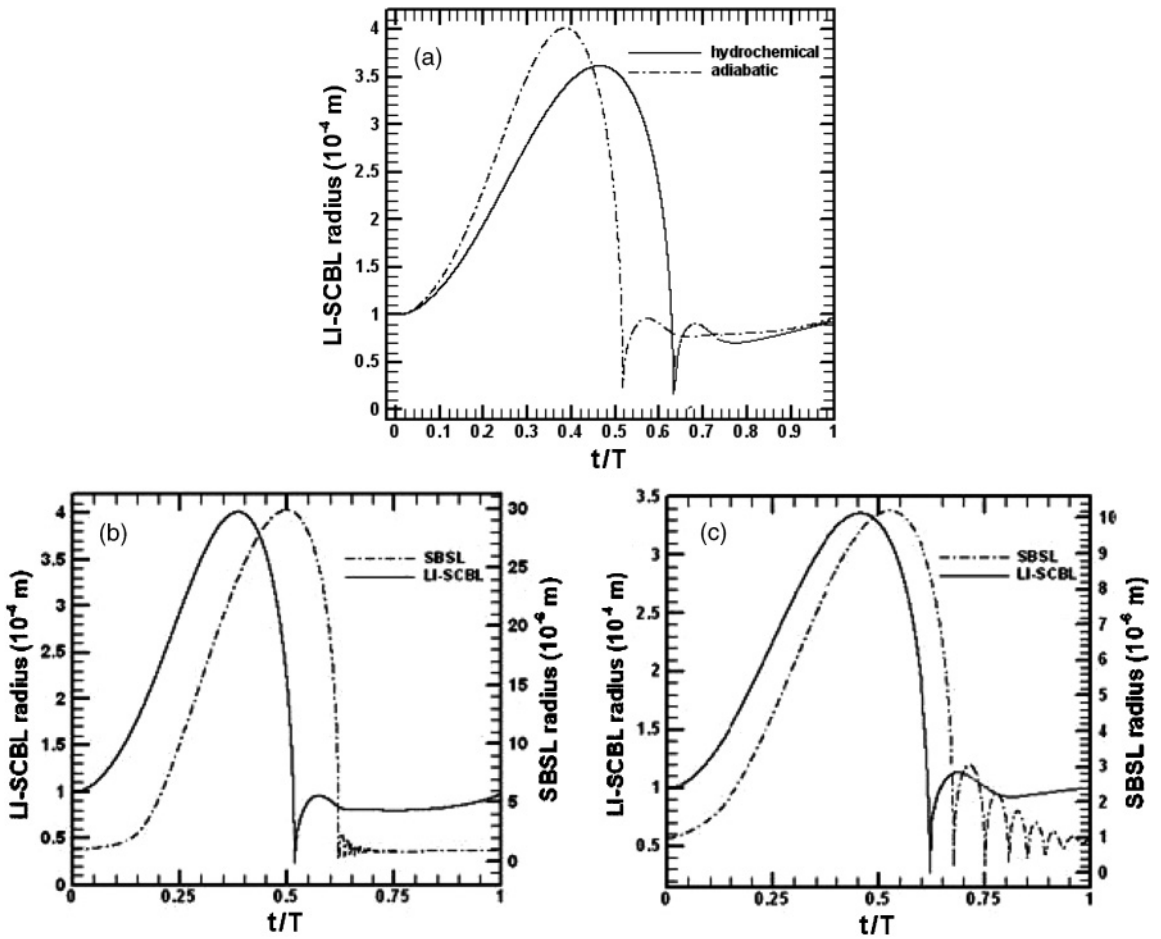

FIG. 8. Comparison of the bubble radius for (a) LI-SCBL in the presence of laser for two models: the quasiadiabatic model (dash-dotted line) and the hydrochemical model (solid line). The bubble radius for SBSL (dash-dotted line) and LI-SCBL in the presence of the acoustic field (solid line) is compared for two models: (b) the quasiadiabatic model and (c) the hydrochemical model for the luminescence parameter regime Fig. 1.

driving pressure amplitudes and ambient bubble radius of $P_a = 1.2$ bars with $R_0 = 0.4 \times 10^{-4}$ m, $P_a = 2$ bars with $R_0 = 1.2 \times 10^{-4}$ m, and $P_a = 3$ bars with $R_0 = 2.1 \times 10^{-4}$ m, and (b) in SBSL for $P_a = 1.5$ bars with $R_0 = 1.3 \times 10^{-6}$ m, $P_a = 1.6$ bars with $R_0 = 2 \times 10^{-6}$ m, and $P_a = 1.7$ bars with $R_0 = 2.5 \times 10^{-6}$ m. By increasing the driving pressure amplitude in LI-SCBL in the presence of the acoustic field, temperature increases from about 2000 to 7000 K, which is more than three times larger. Although the order of temperature in SBSL is more than seven times larger than that in the LI-SCBL in the presence of the acoustic field, increasing the driving pressure amplitude cannot considerably affect the bubble interior temperature. As seen in Fig. 6(b), the temperature varies from about 40 000 K to 47 000 K. The laser effect on the fluid causes a larger bubble interior temperature change compared to that in the SBSL. This diagram shows several peaks for SBSL and this is due to bubble afterbounces induced by the acoustic field.

Figure 7 shows the variation of the bubble interior temperature in the two mentioned situations by various driving pressure amplitudes and proper ambient bubble radius that is presented in Fig. 6 with semilogarithmic scale to indicate the structure.

A comparison is done between quasiadiabatic and hydrochemical models in the bubble induced by laser in the presence of the acoustic field for the bubble radius in Fig. 8. Figure 8(a) indicates the fluctuations of the bubble radius induced by laser in the presence of the acoustic field in one cycle in the luminescence parameter regime as used in Fig. 1 for two models: (i) the quasiadiabatic model (dash-dotted line) and (ii) the hydrochemical model (solid line). One can find the lower bubble radius in the hydrochemical model by considering condensation and evaporation on the bubble wall and the vapor effects, which is about 10% less than the equivalent quantity, by using the quasiadiabatic model for the similar condition. However, the relative difference of the two mentioned models for SBSL and LI-SCBL in the presence of the acoustic field is only 5%. This is presented in Figs. 8(b) and 8(c), where a comparison of the bubble radius for the SBSL and LI-SCBL in the presence of the acoustic field is done for (b) the quasiadiabatic model and (c) the hydrochemical model. The driving parameters are considered the same as for Fig. 1. As can be noticed, the bubble radius difference of the 92% from Fig. 8(b) and 97% from Fig. 8(c) is observed between the SBSL and LI-SCBL in the presence of the acoustic field for the quasiadiabatic model and the hydrochemical model, respectively, which is only 5% and this is half of their absolute difference. As a consequence, using the quasiadiabatic model in this work to show the relative difference of SBSL and LI-SCBL in the presence of the acoustic field is justified.

Figure 9 indicates the variation of (a) total particles and (b) H_2O particles for SBSL and LI-SCBL in the presence of the acoustic field during one cycle in the semilogarithmic scale in the hydrochemical model in the luminescence parameters regime as used in Fig. 1. It should be noted that the left scale chart is based on 10^{14}, which shows the number of particles in LI-SCBL in the presence of the acoustic field, but the right scale chart is based on 10^{11}, which shows the number of particles in SBSL. As seen in Fig. 9, the number of particles

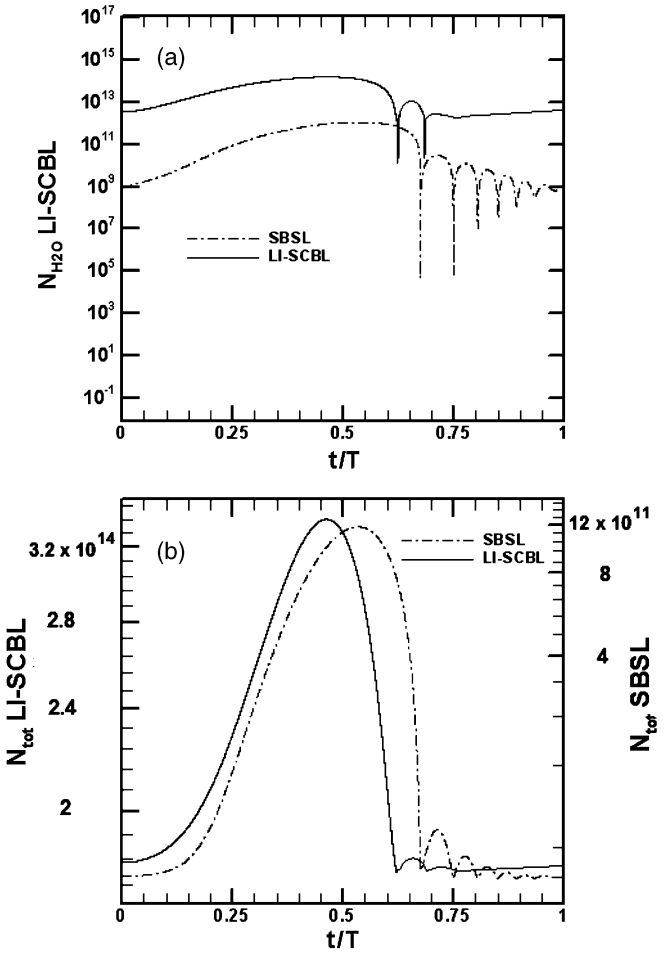

FIG. 9. Comparison of the bubble interior (a) H_2O particles and (b) total particles between LI-SCBL in the presence of the acoustic field and SBSL in logarithmic scale.

in LI-SCBL in the presence of the acoustic field is larger than SBSL. This is due to the larger LI-SCBL bubble volume in the presence of the acoustic field than the one in SBSL. However, the effect of chemical reactions in LI-SCBL in the presence of the acoustic field is less than 10%. Therefore, it can be ignored with good approximation. However, this is more effective in SBSL as shown in Fig. 8. This could be due to the much lower temperature at the collapse time for LI-SCBL in the presence of the acoustic field than one in SBSL. Figure 9 also shows that the number of particles in the bubble increases during the bubble radius expansion and reaches to its maximum value in the maximum bubble radius. During the compression, the particles are removed from the bubble, therefore, the number of particles inside the bubble decreases quickly. At the end of the cycle, the number of particles reaches its initial value.

IV. CONCLUSION

In the present work, the bubble parameters and its evolution induced by laser is completely explained. The bubble radius, the bubble interior pressure, and the temperature in one cycle are investigated and compared with the single-bubble sonoluminescence in the presence of an acoustic field. The main difference between these situations is compressibility

that is shown by the variable speed of sound: $C = \sqrt{dp/d\rho}$. In other words, the compressible fluid induced by laser creates the conditions so that the bubble radius of LI-SCBL in the presence of the acoustic field is larger than that in the SBSL. A comparison is also made between SBSL and LI-SCBL in the presence of the acoustic field with respect to different driving pressure amplitudes. It should be realized that the consistency of these results for LI-SCBL in the presence of the acoustic field with the reported experimental observation for the maximum bubble radius and the maximum interior temperature in the collapse time indicates the reliability of this method for the other mentioned calculated parameters. The obtained results indicate that by increasing the driving pressure amplitude, the bubble radius decreases in both cases but the bubble interior pressure and the related temperature increases. The magnitude of the bubble interior pressure and the temperature in SBSL are much larger than that in the LI-SCBL in the presence of the acoustic field. This is because of the large difference between the maximum and the minimum of the bubble radius in the SBSL with that in the LI-SCBL in the presence of the acoustic field. The magnitudes of the pressure and the temperature in LI-SCBL in the presence of the acoustic field are not as big as those in the SBSL, which is the main reason it would make it less desirable for sonofusion applications. However, the 10^6 times obtained larger bubble volume contains more radiating species in the collapse time, which is an important step forward for obtaining the larger cavity needed for stronger stimulated emission required for the newly proposed SASER applications.

ACKNOWLEDGMENTS

The authors acknowledge the research deputy of Sharif University of Technology for financial support of this project.

[1] R. Mettin, I. Akhatov, U. Parlitz, C. D. Ohl, and W. Lauterborn, Phys. Rev. E **56**, 2924 (1997).
[2] R. Sadighi-Bonabi, N. Rezaee, H. Ebrahimi, and M. Mirheydari, Phys. Rev. E **82**, 016316 (2010).
[3] K. Yasui, Phys. Rev. E **60**, 1754 (1999).
[4] D. F. Gaitan, L. A. Crum, C. C. Church, and R. A. Roy, J. Acoust. Soc. Am. **91**, 3166 (1992).
[5] A. Moshaii and R. Sadighi-Bonabi, Phys. Rev. E **70**, 016304 (2004).
[6] W. C. Moss, D. B. Clarke, and D. A. Young, Science **276**, 1398 (1997).
[7] R. A. Hiller, S. J. Putterman, and K. R. Weninger, Phys. Rev. Lett. **80**, 1090 (1998).
[8] T. J. Matula, J. Guan, L. A. Crum, A. L. Robinson, and L. W. Burgess, Phys. Rev. E **64**, 026310 (2001).
[9] S. Hilgenfeldt, D. Lohse, and W. C. Moss, Phys. Rev. Lett. **80**, 1332 (1998).
[10] G. E. Vazquez and S. J. Putterman, Phys. Rev. Lett. **85**, 3037 (2000).
[11] R. Hiller, K. Weninger, S. Putterman, and B. P. Barber, Science **266**, 248 (1994).
[12] R. G. Holt and D. F. Gaitan, Phys. Rev. Lett. **77**, 3791 (1996).
[13] R. Toegel, S. Luther, and D. Lohse, Phys. Rev. Lett. **96**, 114301 (2006).
[14] M. J. Moran and D. Sweider, Phys. Rev. Lett. **80**, 4987 (1998).
[15] R. Pecha, B. Gompf, G. Nick, Z. Q. Wang, and W. Eisenmenger, Phys. Rev. Lett. **81**, 717 (1998).
[16] M. P. Brenner, D. Lohse, D. Oxtoby, and T. F. Dupont, Phys. Rev. Lett. **76**, 1158 (1996).
[17] I. Akhatov, N. Gumerov, C. D. Ohl, U. Parlitz, and W. Lauterborn, Phys. Rev. Lett. **78**, 227 (1997).
[18] A. Moshaii, R. Sadighi-Bonabi, and M. Taeibi-Rahni, J. Phys.: Condens. Matter **16**, 1687 (2004).
[19] M. Harrison, J. Acoust. Soc. Am. **24**, 776 (1952).
[20] A. Shima, K. Takayama, Y. Tomita, and N. Miura, Acustica **48**, 293 (1981).
[21] F. B. Peterson and T. P. Anderson, Phys. Fluids **10**, 874 (1967).
[22] T. E. McGrath, A. C. Beveridge, and G. J. Diebold, Appl. Phys. Lett. **73**, 1029 (1998).
[23] O. Baghdassarian, B. Tabbert, and G. A. Williams, Phys. Rev. Lett. **83**, 2437 (1999).
[24] A. Vogel, W. Lauterborn, and R. Timm, J. Fluid Mech. **206**, 209 (1989).
[25] K. Nahen and A. Vogel, IEEE J. Quantum Electron. **2**, 847 (1996).
[26] Sh. Eliezer, *The Interaction of High-Power Lasers with Plasmas* (IOP Publishing Ltd., London, 2002).
[27] J. Noack and A. Vogel, IEEE J. Quantum Electron. **35**, 8 (1999).
[28] I. Akhatov, N. Vakhitova, A. Topolnikov, K. Zakirov, B. Wolfrum, T. Kurz, O. Lindau, R. Mettin, and W. Lauterborn, Exp. Therm. Fluid Sci. **26**, 731 (2002).
[29] B. P. Barber, R. A. Hiller, R. Löfstedt, S. J. Putterman, and K. R. Weninger, Phys. Rep. **281**, 65 (1997).
[30] C. D. Ohl, O. Lindau, and W. Lauterborn, Phys. Rev. Lett. **80**, 393 (1998).
[31] A. J. Kent, R. N. Kini, N. M. Stanton, M. Henini, B. A. Glavin, V. A. Kochelap, and T. L. Linnik, Phys. Rev. Lett. **96**, 215504 (2006).
[32] I. V. Volkov, S. T. Zavtrak, and I. S. Kuten, Phys. Rev. E **56**, 1097 (1997).
[33] R. P. Taleyarkhan, C. D. West, J. S. Cho, R. T. Lahey Jr., R. I. Nigmatulin, and R. C. Block, Nature (London) **295**, 1868 (2002).
[34] R. P. Taleyarkhan, C. D. West, R. T. Lahey Jr., R. I. Nigmatulin, R. C. Block, and Y. Xu, Phys. Rev. Lett. **96**, 034301 (2006).
[35] M. P. Brenner, S. Hilgenfeldt, and D. Lohse, Rev. Mod. Phys. **74**, 425 (2002).
[36] R. Sadighi-Bonabi, R. Rezaei-Nasirabad, and Z. Galavani, J. Acoust. Soc. Am. **126**, 2266 (2009).
[37] R. Sadighi-Bonabi, M. Mirheydari, N. Rezaee, and H. Ebrahimi, Phys. Rev. E **84**, 026301 (2011).
[38] H. Y. Kwak and J. H. Na, Phys. Rev. Lett. **77**, 4454 (1996).
[39] K. Yasui, Phys. Rev. E **56**, 6750 (1997).
[40] R. Löfstedt, B. P. Barber, and S. J. Putterman, Phys. Fluids A **5**, 2911 (1993).

[41] L. Gmelin and R. J. Meyer, *Gmelins Handbuch Der Anorganischen Chemie* (Verlag Chemie GmbH, Leipzig, 1985).
[42] J. B. Keller and M. Miksis, J. Acoust. Soc. Am. **68**, 628 (1980).
[43] C. D. Ohl, Phys. Rev. E **61**, 1497 (2000).
[44] R. Gilmore, *The Growth or Collapse of a Spherical Bubble in a Viscous Compressible Liquid*, California Institute of Technology Technical Report No. 26-4 (1952).
[45] E. Lax, *Taschenbunch für Chemikar und Physiker* (Springer-Verlag, Berlin, 1967).
[46] M. Mirheydari, R. Sadighi-Bonabi, N. Rezaee, and H. Ebrahimi, Phys. Scr. **83**, 055403 (2011).
[47] J. O. Hirschfelder, C. F. Curtiss, and R. B. Bird, *Molecular Theory of Gases and Liquids* (Wiley, New York, 1954).
[48] S. Hilgenfeldt, S. Grossman, and D. Lohse, Phys. Fluids **11**, 1318 (1999).
[49] A. Moshaii, Kh. Imani, and M. Silatani, Phys. Rev. E **80**, 046325 (2009).
[50] X. Lu, A. Prosperetti, R. Toegel, and D. Lohse, Phys. Rev. E **67**, 056310 (2003).
[51] M. A. Margulis and I. M. Margulis, Acoust. Phys. **52**, 3 (2006).
[52] M. M. Fyrillas and A. J. Szeri, J. Fluid Mech. **277**, 381 (1994).
[53] S. Hilgenfeldt, D. Lohse, and M. P. Brenner, Phys. Fluids **8**, 2808 (1996).
[54] G. Simon, I. Csabai, Á. Horváth, and F. Szalai, Phys. Rev. E **63**, 026301 (2001).